Long-term expansion and differentiation of adult murine epidermal stem cells in 3D organoid cultures

Kim E. Boonekamp[a,b], Kai Kretzschmar[a,b], Dominique J. Wiener[b,c,d,e], Priyanca Asra[a,b], Sepideh Derakhshan[b,f], Jens Puschhof[a,b], Carmen López-Iglesias[g], Peter J. Peters[g], Onur Basak[b,h,1], and Hans Clevers[a,b,f,1]

[a]Oncode Institute, Hubrecht Institute, 3584 CT Utrecht, The Netherlands; [b]Hubrecht Institute, Developmental Biology and Stem Cell Research, Royal Netherlands Academy of Arts and Sciences and University Medical Centre Utrecht, 3584 CT Utrecht, The Netherlands; [c]Vetsuisse Faculty, Institute of Animal Pathology, University of Bern, 3012 Bern, Switzerland; [d]Dermfocus, Vetsuisse Faculty, Inselspital, Bern University Hospital, 3008 Bern, Switzerland; [e]Department of Veterinary Pathobiology, College of Veterinary Medicine & Biomedical Science, Texas A&M University, College Station, TX 77843; [f]Princess Máxima Center for Pediatric Oncology, 3584 CS, Utrecht, The Netherlands; [g]Maastricht Multimodal Molecular Imaging Institute, Maastricht University, 6229 ER Maastricht, The Netherlands; and [h]Department of Translational Neuroscience, University Medical Center Utrecht Brain Center, Utrecht University, 3584 CG Utrecht, The Netherlands

Contributed by Hans Clevers, October 8, 2018 (sent for review August 29, 2017; reviewed by Salvador Aznar Benitah and Michaela Frye)

Mammalian epidermal stem cells maintain homeostasis of the skin epidermis and contribute to its regeneration throughout adult life. While 2D mouse epidermal stem cell cultures have been established decades ago, a long-term, feeder cell- and serum-free culture system recapitulating murine epidermal architecture has not been available. Here we describe an epidermal organoid culture system that allows long-term, genetically stable expansion of adult epidermal stem cells. Our epidermal expansion media combines atypically high calcium concentrations, activation of cAMP, FGF, and R-spondin signaling with inhibition of bone morphogenetic protein (BMP) signaling. Organoids are established robustly from adult mouse skin and expand over at least 6 mo, while maintaining the basal-apical organization of the mouse interfollicular epidermis. The system represents a powerful tool to study epidermal homeostasis and disease in vitro.

mammalian epidermis | organoids | adult stem cells | interfollicular epidermis

The skin is one of the largest organs of the mammalian body. Its principle functions include prevention from loss of fluid and electrolytes and protection against physical, chemical, and biological insult (1). The uppermost layer of the skin, the epidermis, comprises 3 main compartments: the interfollicular epidermis (IFE), the hair follicle (HF), and the sebaceous gland (SG). The underlying dermis is separated from the epidermis by a basement membrane rich in extracellular matrix proteins (2). The IFE is a stratified epithelium mainly composed of keratinocytes. Proliferative cells reside in the IFE basal layer and are attached to the underlying basement membrane via integrins (3). Differentiating keratinocytes produced in the basal layer are pushed upwards into the suprabasal layers. Upon terminal differentiation, these keratinocytes enucleate and form the cornified envelope, a layer of highly cross-linked dead cells, before being shed off the skin.

Several adult stem cell populations with long-term self-renewal ability have been described in adult murine epidermis (4–6). While these different epidermal stem cell populations maintain cellular turnover during normal homeostasis in a compartmentalized manner, they display remarkable plasticity to contribute to neighboring compartments upon injury (7–10).

Cultures of human epidermal stem cells were successfully established in the mid-1970s by Rheinwald and Green, and crucially depend on a mouse fibroblast feeder layer (11). Because epidermal (burn) injuries and chronic wounds affect millions of patients (12), the culture of human epidermal stem cells as an epithelial layer was further optimized for their use in the clinic (13, 14). Alternative liquid–air interface systems, for example using de-epidermized dermis cultures, allow reconstruction of the tissue architecture for interrogation of basic biological questions (15, 16). Three-dimensional cultures, such as the air–liquid interphase or ex vivo transplants of murine and human epidermis, allow studying exposure to foreign pathogens, but have a limited life span and passageability (17–19). A large amount of knowledge on the biology of mammalian epidermal stem cells has been generated using rodent models (1, 4, 5, 10). However, in culture, murine epidermal keratinocytes spontaneously immortalize, have limited differentiation capacity, and require feeder cells or serum-containing conditions, or can be only solidly established from neonatal skin (20–24). Thus, a long-term in vitro system for the expansion and differentiation of murine epidermal stem cells currently does not exist. Here we present an organoid culture system allowing indefinite (>6 mo) expansion of adult murine epidermal keratinocytes that produce fully differentiated (interfollicular) epidermal structures in vitro.

Results

Establishment of Murine Epidermal Organoid Cultures. As originally established for mouse (25) and human intestinal stem cells (26), epithelial stem cells from multiple adult tissues can be cultured as 3D structures, called organoids, which mimic the cellular

Significance

A vast number of skin pathologies cannot be studied well in vitro because of the lack of a long-term feeder and serum-free culture system for epidermis. Here we develop a long-term culture system for adult murine keratinocytes that is genetically stable over time. Using an organoid-based approach, we establish a 3D culture of murine keratinocytes that resembles the interfollicular epidermis, including proliferative cells in the basal layer and differentiation toward the cornified envelope. As culture models of spontaneously differentiating murine epidermis, these organoids may therefore serve as a platform for studying the basic biology of skin diseases, such as cancer, and their underlying genetic alterations.

Author contributions: K.E.B., K.K., O.B., and H.C. designed research; K.E.B., K.K., D.J.W., P.A., S.D., C.L.-I., and O.B. performed research; K.E.B., K.K., D.J.W., P.A., S.D., J.P., C.L.-I., P.J.P., O.B., and H.C. analyzed data; and K.E.B., K.K., O.B., and H.C. wrote the paper.

Reviewers: S.A.B., Institute for Research in Biomedicine Barcelona; and M.F., University of Cambridge.

Conflict of interest statement: H.C. and K.K. are inventors on patents or patents pending on Lgr5 stem cell-based organoid technology.

Data deposition: The data reported in this paper have been deposited in the Gene Expression Omnibus (GEO) database, https://www.ncbi.nlm.nih.gov/geo (accession no. GSE104521).

[1]To whom correspondence may be addressed. Email: o.basak@umcutrecht.nl or h.clevers@hubrecht.eu.

This article contains supporting information online at www.pnas.org/lookup/suppl/doi:10.1073/pnas.1715272116/-/DCSupplemental.

Published online June 28, 2019.

composition of their respective tissue-of-origin (27). Several culture systems for murine skin epidermis have been established. To circumvent some of their limitations, we designed an organoid culture system for adult murine epidermis. We systematically screened for media components that allow feeder- and serum-free expansion of epidermal keratinocytes. We isolated primary epidermal keratinocytes from mouse telogen back skin, as described by Watt and colleagues (28), and embedded unsorted single cells in basement membrane extract (BME) (Fig. 1*A*). We started from the basic medium utilized for the generation of mouse small intestinal organoids (25), consisting of advanced DMEM/F12 with antibiotics (penicillin/streptomycin), a buffering agent (Hepes), an L-glutamine source (GlutaMAX), B27 supplement (29), and a Rho kinase inhibitor (Y-27632) to inhibit anoikis (25). We enriched this basic medium with additional growth factors based on previously defined conditions for the expansion of epidermal stem cells. First, Wnt/β-catenin signaling is essential for epidermal stem cell self-renewal (30) and the Wnt agonist R-spondin 1 is already a component of the established intestinal organoid medium (25). Second, the extracellular signal-related kinase (ERK)/mitogen-activated protein kinase (MAPK) signaling cascade is activated by epidermal growth factor (EGF) or fibroblast growth factors (FGFs) and stimulates epidermal stem cell proliferation in vitro (31). Third, the signaling pathways of bone morphogenetic protein (BMP) and TGF-β stimulate HF stem cell quiescence (32–34) and are blocked by the respective inhibitors Noggin and A-83-01 (hereafter TGF-βi). Fourth, cyclic adenosine monophosphate (cAMP) increases epidermal keratinocyte expansion in vitro (35) and is activated by Forskolin (36).

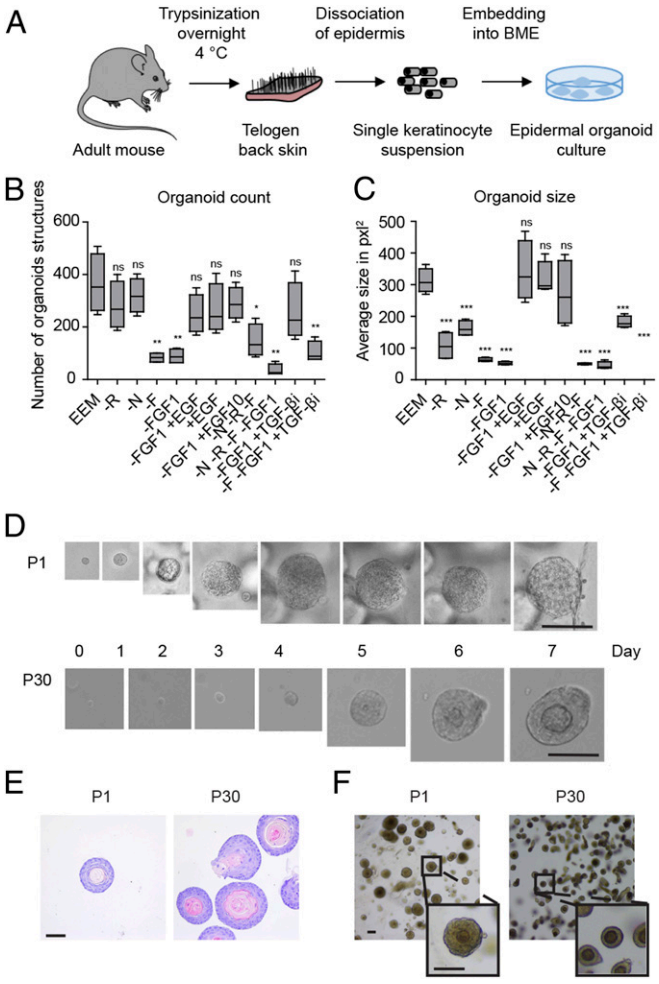

Fig. 1. Establishment of murine epidermal organoid cultures. (*A*) Schematic overview of the tissue processing and organoid culture method. Quantification of organoid-forming efficiency (*B*) and average organoid size (*C*) in the different media. Box plots depict the mean and 25th percentiles ($n = 4$). Student's *t* test, $*P < 0.05$, $**P < 0.01$, $***P < 0.001$, or nonsignificant (ns) $P \geq 0.05$. (*D*) Overview of epidermal organoids forming from single cells within 7 d of culture following initial plating or after long-term passaging (6 mo) (Scale bars, 500 μm). (*E*) H&E stainings of organoids are shown after passage 1 and 30, 7 d after splitting (Scale bars, 100 μm). (*F*) Brightfield images of organoids culture in EEM 7 d after passaging (passages 1 and 30) (Scale bars, 50 μm).

To determine optimal culture conditions, we assessed different combinations of these growth factors. We identified that a defined epidermal expansion medium (EEM) containing Noggin (N), R-spondin 1 (R), Forskolin (F), and FGF1 provides the most optimal growth conditions with many large organoids being generated within 1 wk (Fig. 1 *B* and *C* and *SI Appendix*, Fig. S1*A*). No organoids formed in the absence of all of these factors (–N –R –F –FGF1). Withdrawal of either FGF1 or Forskolin significantly reduced organoid count and size (Fig. 1 *B* and *C*). Removal of Noggin or R-spondin 1 allowed formation of many small organoids, suggesting that both factors are required for organoid expansion (Fig. 1 *B* and *C* and *SI Appendix*, Fig. S1*B*). Culture medium containing either EGF or FGF1 generated proliferative organoids (Fig. 1 *B* and *C* and *SI Appendix*, Fig. S1 *B*, *E*, and *F*), suggesting that EGF and FGF1 do not synergize and can functionally replace each other in culture. FGF1 could be further replaced by FGF10, suggesting that both growth factors may act through FGF receptor 1b activation (37). Culture medium containing TGF-β inhibitor instead of FGF1 allowed the formation of organoids, but resulted in more differentiated organoids with less viability (*SI Appendix*, Fig. S1 *B*, *E*, and *G*). In the absence of FGF1, TGF-β inhibition did not improve organoid count and size, but addition of Forskolin partially restored organoid formation (Fig. 1 *B* and *C* and *SI Appendix*, Fig. S1*B*). Organoids could be maintained at comparable proliferation rates for several passages in culture conditions containing FGF, EGF, or TGF-βi (*SI Appendix*, Fig. S1 *E* and *F*). In conclusion, activation of ERK/MAPK through either FGFs or EGF in combination with BMP inhibition by Noggin, stabilization of Wnt/β-catenin signaling by R-spondin 1, and cAMP activation by Forskolin are essential for formation of murine epidermal organoids.

To investigate the optimal cell concentration for expansion of organoids, we tested different cell-seeding densities. Organoid formation was optimal at 2,500 cells per 10 μL BME drop in a well of a 48-well plate and deteriorated below 1,000 cells per 10 μL of BME (*SI Appendix*, Fig. S1 *C* and *D*). Single-cell suspensions generated organoids (Fig. 1*D*). Compact organoid structures with a keratinizing inner core formed within 1 wk, independent of the passage number, even though the amount of keratinization was higher in later passages (Fig. 1*E*). Organoid cultures could be passaged every 7 d in an approximate ratio of 1 to 4. Murine epidermal organoids were cultured for up to 6 mo while retaining this morphology (Fig. 1*F*).

***Lgr5*, *Lgr6*, and SCA-1 Identify Multiple Sources of Organoids.** We questioned whether different (integrin $\alpha6^+$) epidermal stem and progenitor cell compartments can initiate organoid formation. We and others previously described the existence of HF stem cells marked by leucine-rich repeat-containing G protein-coupled receptor 5 (*Lgr5*) and stem cells in several epidermal compartments marked by *Lgr6* (8, 30, 38–41). While *Lgr5* is highly expressed in the lower HF (Fig. 2*A*), *Lgr6* expression is confined to the upper HF (*SI Appendix*, Fig. S2*A*). Cellular expression of stem cell antigen-1 (SCA-1, encoded by the *Ly6a* gene) marks the infundibulum and the IFE, including the

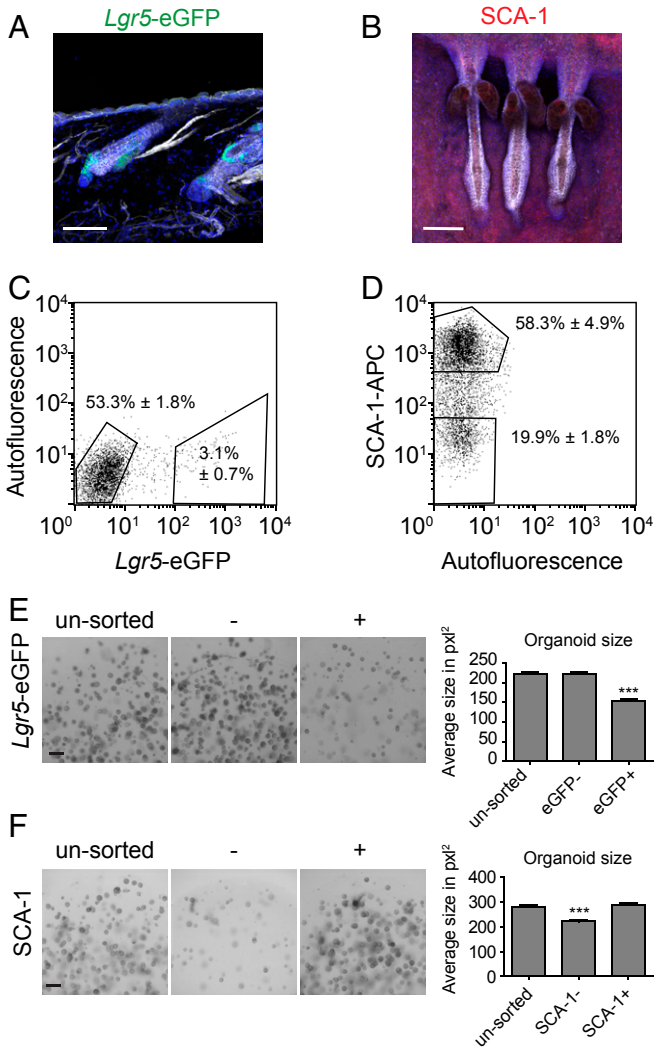

Fig. 2. Organoid establishment from HF and IFE. Maximum projection *z*-stacks of *Lgr5*-eGFP (green) expression in 50-μm-thick frozen sections (*A*) and SCA-1 (red) expression in tail whole mounts (*B*), counterstained for F-actin (gray) and nuclear stain, DAPI (blue) (Scale bars, 100 μm). Flow cytometry plots indicating gating strategy for SCA-1 (*C*) and *Lgr5*-eGFP (*D*). Indicated are mean values ± SD ($n = 2$). (*E*) Brightfield images of organoids derived from cells sorted based on *Lgr5*-eGFP expression and quantification of organoid size (Scale bar, 500 μm). (*F*) Brightfield images of organoid derived from sorted SCA-1$^-$, SCA-1$^+$, and unsorted cells (Scale bar, 500 μm). Quantification of organoid size. Depicted are mean size and SEM ($n = 8$), Student's *t* test, $^{***}P < 0.001$.

respective stem cell populations (Fig. 2*B*). We used our *Lgr5*^{eGFPiresCreERT2} and *Lgr6*^{eGFPiresCreERT2} knockin mouse models (41, 42) as well as SCA-1 immunolabeling to purify *Lgr5*-eGFP$^+$, *Lgr6*-eGFP$^+$, and SCA-1$^+$ keratinocytes (Fig. 2 *C* and *D* and *SI Appendix*, Figs. S2 *B* and *C* and S3). In line with previous reports (38, 40, 43), we found that these keratinocyte subpopulations were enriched for CD49f/ITGA6$^+$ cells (~95%), which is consistent with their basal layer identity (*SI Appendix*, Fig. S3). Similar to unsorted epidermal keratinocytes from wild-type mouse back skin (*SI Appendix*, Fig. S1*B*), individual *Lgr5*-eGFP$^+$ and *Lgr6*-eGFP$^+$, and SCA-1$^+$ stem cells formed organoids within 1 wk (Fig. 2 *E* and *F* and *SI Appendix*, Fig. S2*D*), which could be passaged. However, both the number and the average size of the organoids differed. The SCA-1$^+$ and *Lgr5*-eGFP$^-$ fractions were more efficient in both initiating organoids and forming larger organoids (Fig. 2 *E* and *F* and *SI Appendix*, Fig. S2*D*). In short, while our culture conditions support the maintenance and expansion of multiple epidermal compartments in vitro, IFE and infundibular stem cells are more efficient in performing that task.

Whole-Transcriptome Analysis Identifies Epidermal Organoids as IFE-Like. Multiple combinations of growth factors allowed the initial outgrowth of organoids (Fig. 1 *B* and *C*). To elucidate the differences between these conditions and to reveal the molecular phenotype of the organoids, we performed messenger RNA (mRNA)-sequencing to comprehensively compare the transcriptomes of organoid cultures. We generated libraries from organoids of primary (1 wk) and early (4–7 wk) passages kept under different media compositions. RNA isolated from HFs microdissected from murine back skin during the anagen phase or SCA-1$^+$ IFE cells (further referred to as IFE) sorted from telogen back skin were used as primary tissue control (44). Our dataset consisted of 23 samples covering ~20,000 genes in total (Fig. 3 and *SI Appendix*, Fig. S4).

Hierarchical clustering revealed differences between epidermal organoids and primary tissue controls (Fig. 3*A*). In support, differential gene-expression analysis confirmed the differences between the organoids and IFE (3,084 genes with <0.01 false discovery rate [FDR]) (*SI Appendix*, Fig. S4*A*), and between the organoids and anagen HFs (4,340 genes with <0.01 FDR) (*SI Appendix*, Fig. S4*A*). Genes encoding markers for the basal layer, IFE, HF stem cells, and HF differentiation were expressed in the organoids following the trend found in IFE (Fig. 3*B*). The expression of IFE and infundibulum marker *Ly6a* (encoding SCA-1) and absence of expression of HF stem cell and HF differentiation genes *Lgr5*, *Lef1*, and keratin genes, such as *Krt73* and *Krt71*, in combination implicated an IFE/infundibulum identity of the murine epidermal organoids. The combined expression of basal layer markers *Krt5* and *Itga6* and differentiation marker *Krt10* confirmed that our in vitro system mimics the in vivo epidermal stratified epithelium.

Compared with HFs, organoids had up-regulated epidermal suprabasal marker *Krt6b* (+16.4×) and genes involved in epidermal barrier formation, such as *Sprr2d* (+15.6×) (45) and *Ly6a* (+7.4×). *Ly6a* expression in organoids was similar to that of the IFE (+1.8×). Epidermal basal layer marker *Krt14* (+1.4×) was significantly higher in organoids than IFE, and *Krt5* expression was increased (+4.1×) in organoids compared with anagen HFs, indicating an expansion of basal keratinocytes in culture. Compared with anagen-HFs, organoids had down-regulated the expression of SG marker *Scd1* (-2.0×), as well as HF markers *Cux1* (−3.2×), *Lef1* (−9.4×), *Lgr4* (−2.0×), *Lgr5* (−7.2×), and *Tcf7l2* (expressing TCF4; −1.7×). In addition, genes encoding HF keratins, such as *Krt35* (−12.6×), *Krt71* (−17.1×), and *Krt85* (−14.9×) were robustly down-regulated in cultures compared with HFs. Furthermore, organoids showed down-regulated expression of melanocyte marker *Mitf* (−5.5×) (46).

Next, we asked whether the transcriptome of organoids changed with time. Hierarchical clustering suggested high similarity of primary and early-passage organoids in comparison with the tissue controls (Fig. 3*A*). Differential gene-expression analysis revealed some minor differences between primary and early-passage cultures (668 genes with <0.01 FDR). We found decreased expression of matrix metalloproteinases, such as *Mmp3* (+4.2×) and *Mmp9* (+3.3×), as well as nonepithelial markers *Dkk3* (+5.2×), *Ednra* (+3.1×), and *Thy1* (+3.1×) in early-passage organoids compared with primary cultures. Several cell-type–specific genes, including *Krt1*, *Krt10*, *Krt6a*, *Krt6b*, and *Krt15* did not change significantly, suggesting that the cell-type composition is not altered upon short-term culture.

We subsequently asked whether media composition significantly affected gene expression in culture. Overall, major signaling pathway components were similarly expressed in organoids and

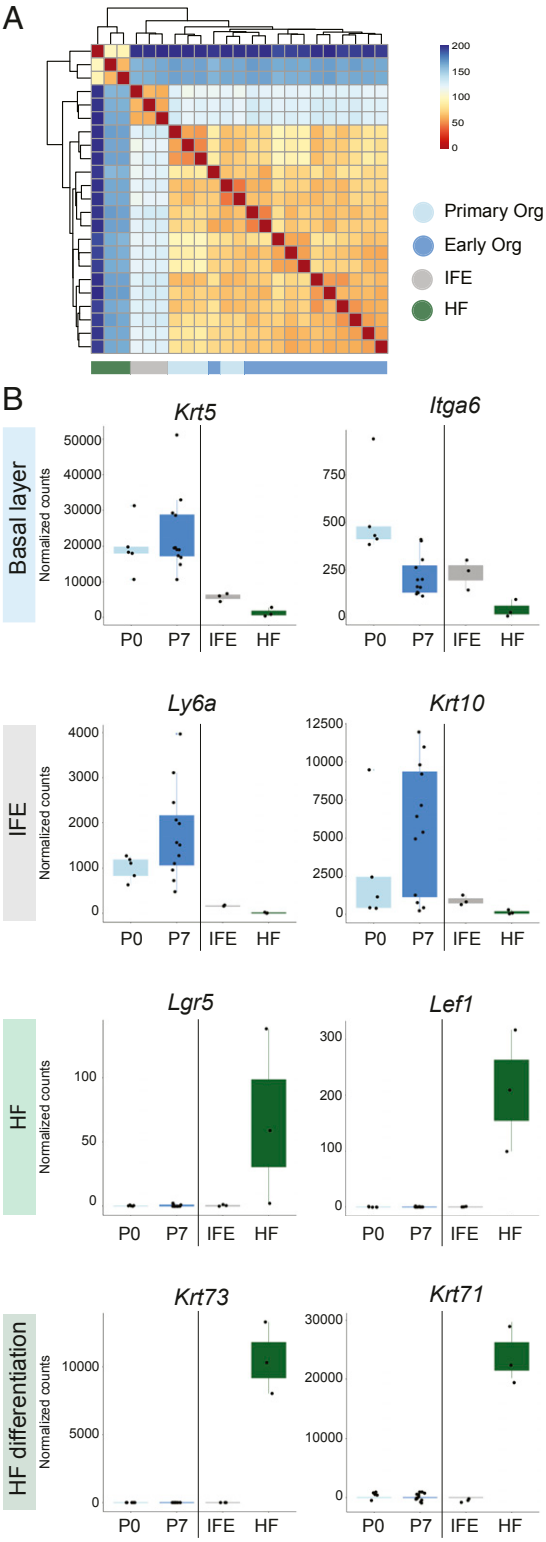

Fig. 3. Whole-transcriptome analysis reveals molecular features of epidermal organoids. (*A*) Hierarchical clustering of gene-expression profiles of anagen HFs, SCA-1^{+}–sorted IFE cells, and primary (P0) and early-passage organoids (~P7). (*B*) Boxplots representing normalized counts of markers specific for either the basal layer, the IFE, HFs, or HF differentiation. Dots represent individual data points. Samples are annotated on the *x* axis, where P0 represents primary organoids (n = 5), ~P7 is early-passage organoids (n = 12), IFE is SCA-1^{+}–sorted cells (n = 3), and HF is anagen-HF (n = 3).

tissue controls, albeit with slightly lower expression of BMP signaling components in organoids (*SI Appendix*, Fig. S4*B*). Consistent with their comparable organoid-forming capacity (Fig. 1*B*), cultures with either FGF1 or FGF10 displayed almost identical gene-expression patterns (1 gene with <0.01 FDR), suggesting that they are indeed interchangeable (*SI Appendix*, Fig. S4*C*). Addition of either FGF1 or FGF10 to the medium triggered a slight change in gene expression (135 genes with <0.01 FDR). Addition of Forskolin (42 genes with <0.01 FDR) triggered only minimal changes in the gene-expression pattern, even though it greatly enhanced organoid growth. This was consistent with similar organoid morphology observed under mentioned culture conditions (*SI Appendix*, Fig. S1 *G*). Addition of TGF-βi induced the highest number of, yet still minor, changes (378 genes with <0.01 FDR) (*SI Appendix*, Fig. S4*B*). The most prominent classes of genes down-regulated by TGF-β inhibition were extracellular matrix proteins, such as *Col4a1* (−4.3×), *Col4a2* (−3.9×), *Sparcl1* (−5.0×), as well as *Tgfb3* (−4.0×) and *Spon2* (−3.0×). While most cell-type–specific markers remained unchanged, we observed a decrease in *Krt14* (−1×) expression at the expense of *Krt15* (+2.4×). None of the culture conditions resulted in significant changes in expression of *Ly6a*. Thus, organoids grown under different media formulations remain very similar, with a slight decrease in basal cell (BC) markers upon TGF-β inhibition.

In conclusion, molecular profiling demonstrated that murine epidermal organoids transcriptionally resemble IFE despite the influence of small changes in media composition and remain transcriptionally stable in short term culture.

Long-Term Expansion of Epidermal Organoids. Culture conditions that support short-term growth of organoids were comparable in maintaining an IFE-like phenotype. Thus, we further cultured organoids in EEM (N/R/F/FGF1) and obtained long-term stable growth (Fig. 1 *E* and *F*). To characterize organoids collected after long-term culturing, we first isolated RNA from organoids of early (~passage [P]5) mid (~P12), and late passages (~P20), as well as keratinocytes cultured on a feeder layer (28), and performed qPCR (Fig. 4*A*). Although robustly expressed, we did not find significant differences in expression of markers of proliferation, the basal layer, and differentiation between different passages of organoid lines (Fig. 4*A*). While we saw a transient increase in *Krt14* expression in early passages and a decrease in *Mki67* expression in the long run, neither were statistically significant (Fig. 4*A*). The HF stem cell marker *Cd34* was expressed in organoids at low, yet comparable levels to control keratinocytes (Fig. 4*A*). In addition, the marker of IFE and the HF infundibulum *Ly6a* was expressed at very high levels in culture, peaking at the latest passage analyzed (Fig. 4*A*), in line with our transcriptome data showing that epidermal organoids were enriched for *Ly6a* mRNA transcripts (Fig. 3*B*). We further found elevated levels of differentiation markers *Krt10* and *Flg1* (encoding Filaggrin1), which were highly expressed in the early passages (Fig. 4*A*).

We next performed immunohistochemistry on paraffin sections prepared from early- (~P5) and late-passage (~P30) organoids cultured in EEM, as well as control back skin tissue to confirm expression of key markers at the protein level. We found strong immunoreactivity against the proliferation marker KI67 in the basal layer of the organoids irrespective of passage number (Fig. 4*B*). In addition, suprabasal layers of the organoids were positive for the early differentiation markers KRT1 and KRT6A, as well as for the marker of terminal differentiation and keratinization Loricrin (Fig. 4*B*). Consistent with our transcriptome analysis of early-passage organoids, Loricrin was expressed at the protein level in passaged organoids indicating de novo differentiation in both early- and late-passage organoids. Immunofluorescence staining of organoid whole mounts showed that the

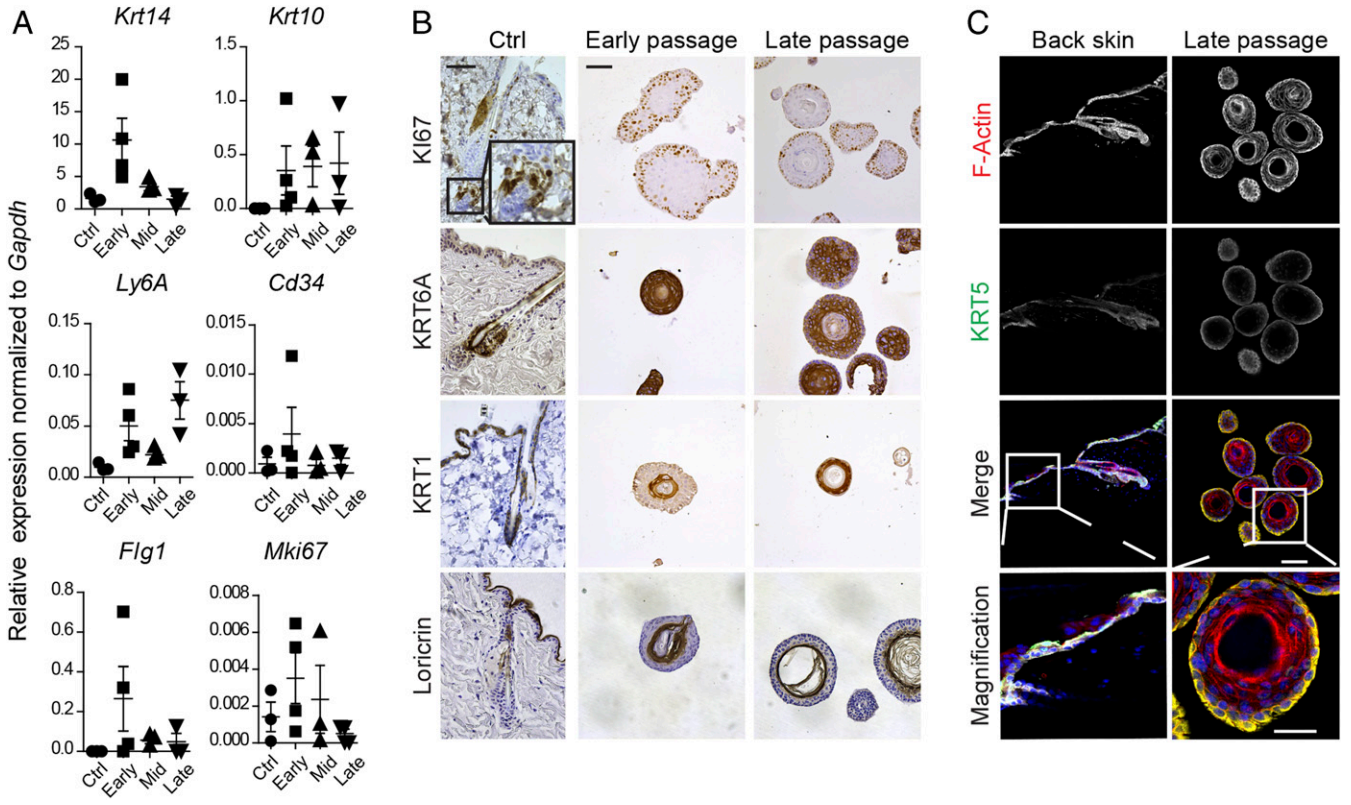

Fig. 4. Characterization of murine epidermal organoids. (*A*) qPCR analysis of organoids normalized to keratinocytes. Dot plots representing gene expression of *Krt14*, *Krt10*, *Flg1*, *Ly6a*, *Cd34*, and *Mki67* relative to *Gapdh*. Mean ± SEM (n = 3–4). Ctrl (P1 2D grown keratinocytes), early passage (~P5), mid passage (~P12), and late passage (~P20). All expression changes are ns ($P \geq 0.05$). (*B*) Immunohistochemical stainings of paraffin-embedded organoids and skin tissue. Representative images of KI67, KRT1, KRT6A, and Loricrin immunoreactivity in control back skin, and early-passage (~P5) and late-passage (~P30) organoids [Scale bars, 50 μm (tissue) and 100 μm (organoids)]. (*C*) Immunofluorescence stainings of whole mount prepared from organoids. Representative images of stainings for KRT5 expression in organoids at passage 30 compared with frozen sections of back skin, counterstained for F-actin (red) and nuclear stain, DAPI (blue) (Scale bars: 100 μm; 50 μm for the magnifications).

late-passage organoids expressed the basal layer marker KRT5 (Fig. 4*C*).

It has previously been reported that cultured murine keratinocytes senesce over time, immortalize through oncogenic mutations, or acquire increased chromosome numbers (20–22). We therefore performed karyotyping on late-passage organoids (~P30). Analysis of 2 independent cultures showed the presence of 40 chromosomes per metaphase spread, suggesting long-term genomic stability in vitro (*SI Appendix*, Fig. S5*A*). To quantify the number of actively cycling cells (in S-G_2-M phases) in our cultures over time, we flow-sorted single cells incubated with the DNA-label DAPI for subsequent cell-cycle analysis. Approximately 30% of keratinocytes in both early- and late-passage organoids were actively cycling, as opposed to 10% in freshly isolated keratinocytes (*SI Appendix*, Fig. S5*B*), demonstrating that our organoids are enriched for proliferative epidermal cells. Next, we evaluated the percentage of differentiated (cornified) organoids over different passages in our cultures by assessing positivity for eosin. This analysis revealed that 41.3 ± 2.0% (mean ± SEM) organoids established from primary keratinocytes were eosin$^+$, while early-passage (P6) and late-passage (P25) organoid cultures contained, 26.4 ± 2.3% and 20.7 ± 2.0% eosin$^+$ organoids, respectively (*SI Appendix*, Fig. S5*C*).

We then performed RNA sequencing on 6 late-passage organoid cultures and compared the whole-transcriptome expression levels to the above-described dataset. Hierarchical clustering suggested high similarity of primary, early-, and late-passage organoids and IFE, while HFs clustered apart (*SI Appendix*, Fig. S6*A*). Principle component analysis revealed that overall, the transcriptome of organoids remained similar over time with a slight change in transcriptome upon long-term passaging (*SI Appendix*, Fig. S6*B*). Continuous expression of *Ly6a* (and other key genes), demonstrated that late-passage organoids molecularly remain IFE-like over time (*SI Appendix*, Fig. S6*C*), despite the presence of differentially expressed genes upon passaging (*SI Appendix*, Fig. S6*E*). Gene ontology term analysis of the top 500 differentially expressed genes in each direction between primary and early-passage organoids and late-passage organoids did not implicate changes in epidermal specific programs (*SI Appendix*, Fig. S6 *F* and *G*).

Finally, we performed colony-forming efficiency (CFE) assays as following the gold standard protocol published by Jensen et al. (28) to confirm that our organoid culture retained murine epidermal stem cells long term. Keratinocytes from late-passage organoid cultures subjected to CFE assays generated holoclones containing typical cobblestone-like epidermal stem cells (Fig. 5 *A*–*C*). However, the average number of colonies almost doubled from primary organoid cultures to late-passage organoids (Fig. 5*D*), suggesting that our culture system enriches for colony-forming cells long term. Collectively, these data demonstrate that the proliferative capacity of murine epidermal stem cells is retained long term in the in vitro organoid system, while their ability to differentiate into IFE-like structures is similarly maintained.

Murine Epidermal Organoids Are Amenable to Genetic Manipulation. Murine epidermal stem cells are widely used to study the biology of mammalian epidermis (1, 4, 5, 10). We therefore aimed to test whether murine epidermal organoids are amenable to genetic

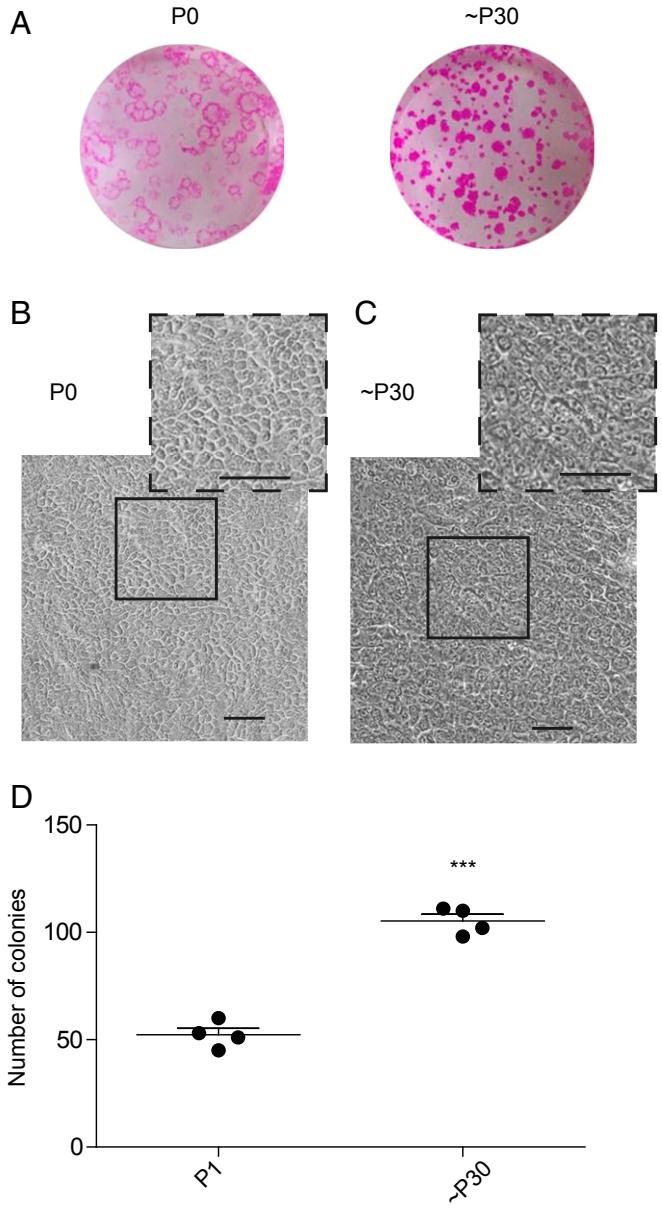

Fig. 5. CFE assays show long-term maintenance of murine epidermal stem cells. (*A*) Representative images of the CFE assay of P0 and ~P30 organoid lines grown for 14 d after start of the culture, stained with 1% Nile blue, 1% Rhodamin B ($n = 2$), micrographs represent overview images of individual wells of a 6-well plate at approximately 1× magnification. (*B*) Representative brightfield images of 2D colonies at day 14 for P0 (Scale bars, 100 μm). (*C*) Representative brightfield images of 2D colonies at day 14 for P30 (Scale bars, 100 μm). (*D*) Quantification of the average number of colonies per well based on technical duplicates and biological duplicates ($n = 4$). Student's *t* test, $***P < 0.001$.

manipulation. We first attempted to introduce an eGFP expression vector by standard Lipofectamin-2000 transfection. However, only very few transfected cells survived. We next introduced lentiviral expression vectors by transduction (*SI Appendix*, Fig. S7*A*). Single cells derived from organoids transduced with a construct encoding Neon-tagged histone H2B (pLenti-H2B-neon-Puro) showed a robust transduction efficiency of about 10% 4 d after passaging (*SI Appendix*, Fig. S7*B*). After puromycin-based selection, we used the H2B-mNeonGreen–tagged organoids for imaging and assessed cell divisions in vitro following a previously published protocol (*SI Appendix*, Fig. S7*C*) (47). We confirmed normal cell division in late-passage organoids.

CRISPR–Cas9 genome editing is an elegant and efficient way to introduce genetic alterations into mammalian cells (48). We therefore tested whether genes-of-interest can be targeted murine epidermal organoids using CRISPR–Cas9 technology. We first introduced a lentiviral iCas9-FLAG expression vector by transduction (Fig. 6*A*). Subsequently, organoid lines stably expressing inducible Cas9 served as a platform to introduce gene knockouts (KO) for desmoplakin (*Dsp*), a gene that is mutated in multiple diseases, including skin fragility-wooly hair syndrome (49). Using 2 different single-guide (sg)RNA sequences, we successfully generated homozygous KO organoid clones lacking expression of *Dsp* mRNA (Fig. 6 *B* and *C* and *SI Appendix*, Fig. S8*A*). We then analyzed epidermal marker genes by qPCR (*SI Appendix*, Fig. S8 *A* and *B*). While expression of the basal layer marker gene *Krt14* and proliferation marker gene *Mki67* remained similar between the *Dsp* KO organoids and control organoids, expression of differentiation marker genes *Krt10*, *Filaggrin*, and *Involucrin* were significantly down-regulated in the *Dsp* KO organoids.

Transmission electron microscopy (TEM) revealed clear morphological changes upon genetic ablation of *Dsp*. Semithin sections stained with Toluidine blue showed clear multilayered organization of wild-type organoids (Fig. 6 *D*, *Left*), while mutant organoids (Fig. 6 *D*, *Right*) appeared less organized and less cornified. The multilayered phenotype in wild-type organoids was further confirmed by high-resolution TEM (Fig. 6 *E*, *Left*), with the BC located on the outside of the organoids. While the spinous layer (SP), granular layer (GR), keratin granules (KG), and stratum corneum (SC) were found toward the center of the organoids. The mutant organoids lacked this clear organization (Fig. 6 *E*, *Right*). Magnifications of the organoids (*SI Appendix*, Fig. S8 *C–E*, *G*, and *H*) showed less attachment between the cells in the mutant (*SI Appendix*, Fig. S8 *D*, *Bottom*, and *H*), altered adherens junction, desmosome patterning (*SI Appendix*, Fig. S8 *E*, *Bottom*), and atypical organization of the GR (*SI Appendix*, Fig. S8 *E*, *Bottom*).

Brightfield images as well as H&E stainings and stainings for KI67 and KRT10 (Fig. 6*G*) confirmed a similar phenotype in the *Dsp* KO organoids to that described for *Dsp* KO mice in vivo (50). Similarly, *Dsp* KO organoids showed altered polarization of KRT5 within basal layer cells consistent the *Dsp* KO mice phenotype (*SI Appendix*, Fig. S8*F*) (51). As a proof-of-concept, these experiments demonstrated that murine organoids may serve as a platform for gene tagging and gene editing in a self-renewing multilayered epithelium in vitro.

Discussion

In this study, we describe the establishment of a long-term murine 3D keratinocyte culture system. We show that these cultures are genetically stable and feeder- and serum-independent and grow in atypically high-calcium conditions long term. We demonstrate that these organoids can be maintained up to 6 mo retaining their clonogenic potential (as assessed using CFE assays) and their ability to differentiate. Hence, these murine epidermal organoid cultures serve as a model to study adult epidermal homeostasis and disease in vitro.

While culture of murine keratinocytes has been widely reported, these approaches are typically hampered by at least one of the following features: spontaneous immortalization, dependence on feeder cells, and serum or incomplete differentiation, or limited establishment from adult tissue (20–24). With the current culture system, we show the presence of proliferative basal layer cells and differentiation toward the cornified envelope. We find that organoids display an IFE-signature, thus representing a potentially useful tool to study epidermal diseases including blistering diseases, such as pemphigus vulgaris (52).

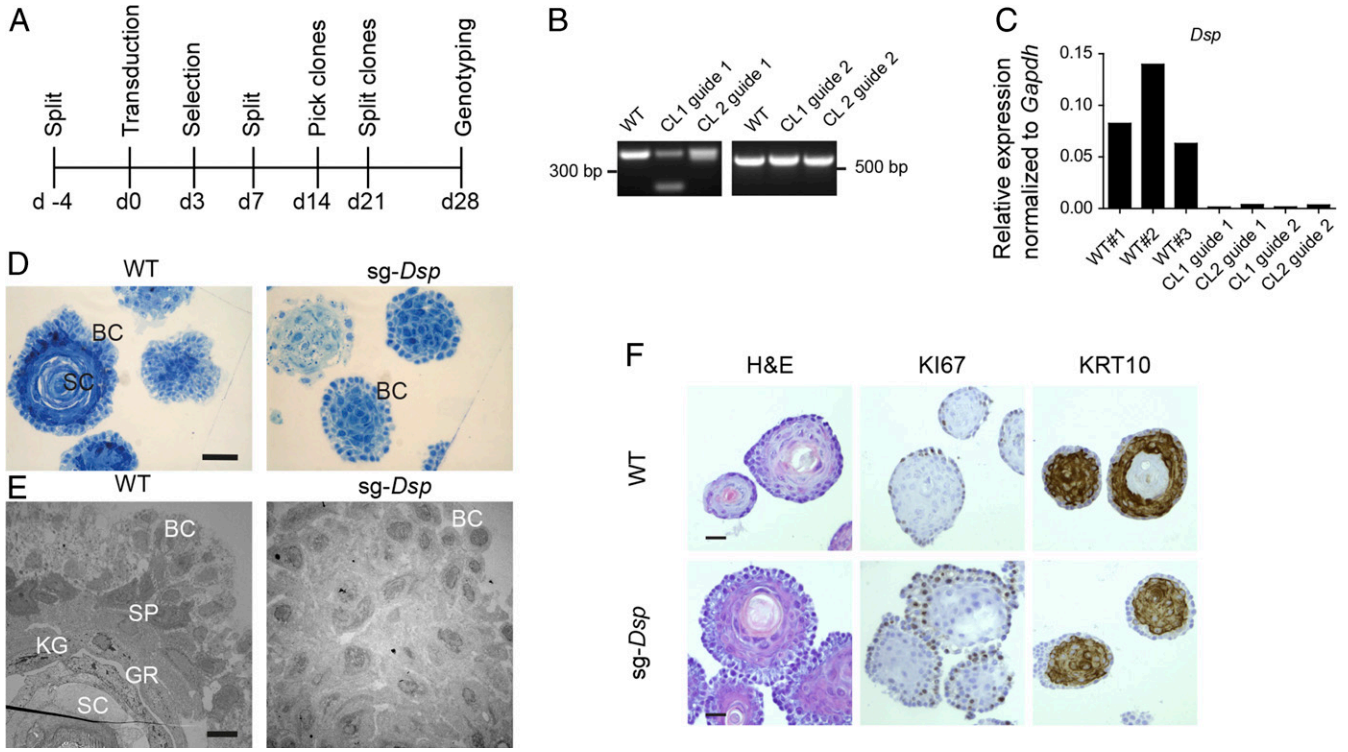

Fig. 6. Genetic alteration of desmoplakin in murine epidermal organoids. (*A*) Time-line of genetic manipulation of murine skin organoids using a lentiviral CRISPR–Cas9 approach. (*B*) Genotyping of clonal organoid lines transduced with two different sgRNAs. (*C*) mRNA expression of *Dsp* normalized to *Gapdh* for 3 wild-type lines and 4 *Dsp* KO clones. (*D*) Semithin sections stained with Toluidine blue to show overall morphology (Scale bar, 50 μm). (*E*) Ultrathin sections in TEM images of wild-type (*Left*) and *Dsp* KO organoids (*Right*) (Scale bar, 10 μm). (*F*) Sections of paraffin-embedded organoids stained with H&E or for KI67 or KRT10 (Scale bars, 100 μm).

Established model systems, such as mouse models, 2D-feeder–based cultures, or air–liquid interphase cultures provide complementary systems that allow studying of interactions with pathogens originating from the outside world.

Aberrations of intercellular adhesions, called desmosomes, by mutations in desmosomal genes, such as *Dsc3* (Desmocollin 3), result in intraepidermal blistering, as in pemphigus vulgaris patients (53). As a proof-of-principle, we generated homozygous *Dsp* KOs using CRISPR–Cas9 technology and characterized the phenotype in vitro. Because organoids serve as versatile tools allowing for disease modeling, targeted gene editing, drug testing, transcriptome analysis, and studying of interactions, such as those of host–microbe (27), a wide range of new possibilities for basic and translational research opened up.

Our culture system contains high calcium, originating from the advanced DMEM/F12 basic medium. Traditionally, mouse keratinocytes are expanded in low calcium, whereas an increase in calcium induces their differentiation in culture (28). Thus, although we observe epidermal organoid differentiation, we simultaneously show prominent proliferation of BCs, indicating that keratinocytes do not only "unconditionally" differentiate under high calcium levels in vitro.

We show highly efficient organoid formation of SCA-1$^+$ and *Lgr5*-eGFP$^-$ keratinocytes, therefore enriched for non-HF (stem) cells. However, we also demonstrate that direct establishment of organoids from HF cells (SCA-1$^-$ cells) or HF stem cells (*Lgr5*-eGFP$^+$ cells). We hypothesize that at least some of the stem cells present in *Lgr5*-eGFP$^+$ and SCA-1$^-$ pool of cells retain the ability to adopt an IFE-like fate. This is indicative of plasticity of cellular identity, a phenomenon already known to occur upon skin wounding or when keratinocytes are transplanted in skin reconstitution assays (7–10). Using single-cell transcriptome analysis of murine epidermis, Kasper and colleagues (54) recently showed that the various epidermal stem cell populations share a set of common genes. For example, HF stem cells express core genes of IFE differentiation, suggesting that differentiation toward the IFE lineage may be the default state of epidermal differentiation. In agreement with our observation, this suggests that all epidermal stem cells—irrespective of location in vivo—may therefore differentiate toward cornifying epidermis when placed in culture. Hence, to generate other epidermal compartments, such as HFs or SGs in vitro, more research is required into the signals required to maintain these stem cell populations and to activate their lineage-specific differentiation program.

Methods

A detailed description of materials and methods can be found in *SI Appendix, SI Materials and Methods*.

Mice. Wild-type C57BL/6 mice at 8–18 wk of age were used, unless stated otherwise. Generation and genotyping of the *Lgr5*^{eGFPiresCreERT2} and *Lgr6*^{eGFPiresCreERT2} knockin mouse models are described elsewhere (41, 42). All mice were collected under experimental protocols approved by the Hubrecht Institute Animal Welfare Body within a project license granted by the Central Committee Animal Experimentation of the Dutch government.

Murine Epidermal Keratinocyte Isolation and Culture. Epidermal keratinocytes were isolated from telogen back skin collected from 8- to 18-wk-old mice, as previously described (28, 44). Viable keratinocytes were plated at a density of 2,500 cells per 10 μL BME (Cultrex) drop. Cells were cultured in EEM consisting of advanced DMEM/F12 (Gibco) supplemented with penicillin/streptomycin (100 U/L; Gibco), Hepes, (10 mM; Gibco), GlutaMAX (1×; Gibco), B27 supplement (50× stock; Gibco), *N*-Acetylcysteine-1 (1 mM; Sigma-Aldrich), Noggin-conditioned medium (5%, in-house), R-spondin 1-conditioned medium (5%, in-house, derived from 293T-HA-RspoI-Fc cells provided

by Calvin Kuo, Stanford University, Stanford, CA), acidic FGF1 (100 μg/mL; Peprotech), Heparin (0.2%; Stemcell Technologies), Forskolin (10 ng/mL; Tocris), Rho kinase inhibitor (Y-27632; 10 μM; Sigma-Aldrich), and Primocin (500× stock; Invivogen). Additional components tested include FGF10 (100 μg/mL; Peprotech), TGF-β inhibitor (A-83-01; 2 μM; Tocris), and EGF (50 ng/mL; Invitrogen). Upon seeding or passaging, medium was refreshed every 3–4 d. Organoid cultures were passaged every 7 d in an approximate ratio of 1 to 4 at a density of 2,500 viable cells per 10-μL BME drop. Organoid cultures were stored long term in −80 °C or in liquid nitrogen. Two-dimensional feeder layer-dependent culture of murine epidermal keratinocytes was described elsewhere (28). Further details are given in *SI Appendix, SI Materials and Methods*.

Organoid-Forming Efficiency Assays. Organoid-forming efficiency was determined by quantification of organoid numbers and size. In brief, 8-bit binary images of whole organoid drops were analyzed with the ImageJ (NIH) images using the "analyze particles" option set to the following parameters: size, 25-infinite and circularity, 0.5–1.0 ($n = 4$). CellTiter-Glo luminescent cell viability assays (Promega) were used to assess organoid cell viability ($n = 4$).

Organoid-Forming Capacity of Sorted Keratinocytes. Back skin from wild-type C57BL/6 mice and *Lgr5*^{eGFPiresCreERT2} and *Lgr6*^{eGFPiresCreERT2} knockin mice in telogen were dissociated into single cells. Single cells were sorted on a BD FACSJazz. Wild-type keratinocytes were stained with anti–SCA-1 conjugated APC primary antibody (clone D7, eBioscience, 17-5981-81). Postsorting, cells were plated at a density of 5,000 cells per 10 μL BME. One-week after seeding, organoid-forming capacity was assessed by quantification of organoid numbers and size, as described earlier. Eight replicative measurements were pooled per condition and mean and SEM were calculated using GraphPad Prism (biological $n = 2$, technical $n = 4$).

Determination of the Percentage of CD49f/ITGA6$^+$ and CD34$^+$ Cells. Back skin from wild-type C57BL/6 mice and *Lgr5*^{eGFPiresCreERT2} and *Lgr6*^{eGFPiresCreERT2} knockin mice in telogen were dissociated into single cells. Wild-type keratinocytes were stained with anti–SCA-1 conjugated APC primary antibody (clone D7, eBioscience, 17-5981-81). Keratinocytes isolated from *Lgr5*^{eGFPiresCreERT2} mice were stained with anti-CD34 (Clone RAM34, BD Biosciences, 560230). All cells were stained with anti-CD49f (Clone GoH3, BD Biosciences, 555736). Single cells were sorted on a BD FACSJazz. Ten thousand cells per condition were analyzed using FlowJo software. Two biological replicative measurements were pooled per condition and mean and SEM were calculated using GraphPad Prism.

Immunohistochemistry and Immunofluorescence. Isolated back skin or organoids were fixed in 4% formaldehyde and embedded in paraffin wax using standard protocols. Isolated back skin was embedded in optimal cutting temperature medium (Leica) for frozen sections and organoids for whole-mount staining were stored in PBS containing sodium azide at 4 °C until further use. Stainings of paraffin sections, frozen sections, tail whole mounts, and organoid whole mounts are described in *SI Appendix, SI Materials and Methods*.

qPCR and mRNA Sequencing. Total RNA was extracted from microdissected anagen HFs from primary tissue using TRIzol (Ambion). RNA representative of the IFE was extracted from SCA-1$^+$ basal layer cells sorted from telogen back skin using TRIzol (Ambion). To isolated IFE-specific cells from telogen back skin, we applied the sorting strategy, as shown in *SI Appendix*, Fig. S3*A*, followed by selection of CD49f$^+$ cells and subsequent gating of SCA-1$^+$ cells seen in *SI Appendix*, Fig. S3*D*. Total RNA was extracted from organoids using the RNeasy Mini Kit (Qiagen) according to the manufacturer's protocol and processed for qPCR or mRNA-sequencing. qPCR was performed using iQTM SYBR Green Supermix (Bio-Rad) following the manufacturer's instructions. Messenger RNA-sequencing was performed using the CEL-Seq2 method (55, 56). Primary passage organoids were harvested at 7 d after initial organoid establishment (P0d7), early-passage organoids at ∼P7d7, and late-passage organoids were harvested at ∼P26d7 and isolated with the RNeasy mini kit or viable cells were sorted into TRIzol and RNA was extracted using chloroform-based protocol following standard procedure. A full description of qPCR, calculations and mRNA-sequencing can be found in *SI Appendix, SI Materials and Methods*.

Determination of Cornification. The percentage of cornification within a culture was determined by scoring the percentage of eosin$^+$ organoids over the total number of organoid in H&E-stained sections of paraffin-embedded organoids ($n = 4$–7).

CFE Assay. CFE assays were essentially performed following a previously published protocol (28); 5,000 cells were seeded per well. A full description of the CFE assays can be found in *SI Appendix, SI Materials and Methods*.

Organoid Transduction. Organoids were grown until day 4 postpassaging after which cells were trypsinized to single cells or small organoid clumps. Cells transduced with H2B-mNeonGreen (pLV-H2B-mNeonGreen-ires-Puro). For the CRISPR–Cas9 approach, stably expressing FLAG-iCas9-Puro lines were generated by lentiviral transduction. pCW-Cas9 was a gift from Eric Lander, Broad Institute, Massachusetts Institute of Technology (MIT), Cambridge, MA and David Sabatini, Whitehead Institute for Biomedical Research, MIT, Cambridge, MA (Addgene plasmid #50661) (57). Then, stably expressing iCas9 lines served as basis for lentiviral transduction with 2 different sgRNAs targeting the *Dsp* gene (*SI Appendix*, Table S2). *Dsp* sgRNAs were cloned into lentiGuide-blast (cloned from LentiGuide-Puro). lentiGuide-Puro was a gift from Feng Zhang, Broad Institute, MIT, Cambridge, MA (Addgene plasmid #52963) (58). A full description of transduction of murine skin organoids can be found in *SI Appendix, SI Materials and Methods*.

Electron Microscopy. For TEM, organoids were either grown according to standard procedure until the time of fixation or grown on specific planchettes for 1 d before cryofixation. A full description of electron microscopy procedures can be found in *SI Appendix, SI Materials and Methods*.

Statistics. Significance was determined using unpaired Student's *t* tests performed in GraphPad Prism or Microsoft Excel.

ACKNOWLEDGMENTS. We thank Joep Beumer for advice and critical reading of the manuscript, as well as contributions in the early stages of the project; Wilma Hoevenaar for imaging of the H2B-mNeonGreen–transduced organoids; Maaike van den Born and Johan H. van Es for help with animal procedures; Reinier van den Linden for and Stefan van der Elst help with flow cytometry; the Utrecht Sequencing Facility (USEQ) for sequencing; Anja van de Stolpe and Philips Research for their contributions to the project; the technical staff of the Microscopy CORE Lab of M4I Nanoscopy in Maastricht University and Willine van de Wetering for all their support in microscopy; and Anko de Graaff and the Hubrecht Imaging Center for help with imaging. H.C. gratefully acknowledges financial support from the Swiss National Science Foundation (Sinergia Grant CRSII3 160738-1) and the Netherlands Organization for Scientific Research (NWO-ZonMW, 114021012). This work is part of the Oncode Institute, which is partly financed by the Dutch Cancer Society and was funded by the gravitation program CancerGenomiCs.nl from the Netherlands Organization for Scientific Research (NWO). K.K. is a long-term fellow of the Human Frontier Science Program Organization (LT771/2015) and was the recipient of a VENI grant (NWO-ZonMW, 016.166.140).

1. C. Blanpain, E. Fuchs, Epidermal homeostasis: A balancing act of stem cells in the skin. *Nat. Rev. Mol. Cell Biol.* **10**, 207–217 (2009).
2. F. M. Watt, H. Fujiwara, Cell-extracellular matrix interactions in normal and diseased skin. *Cold Spring Harb. Perspect. Biol.* **3**, a005124 (2011).
3. P. H. Jones, F. M. Watt, Separation of human epidermal stem cells from transit amplifying cells on the basis of differences in integrin function and expression. *Cell* **73**, 713–724 (1993).
4. T. Schepeler, M. E. Page, K. B. Jensen, Heterogeneity and plasticity of epidermal stem cells. *Development* **141**, 2559–2567 (2014).
5. K. Kretzschmar, F. M. Watt, Markers of epidermal stem cell subpopulations in adult mammalian skin. *Cold Spring Harb. Perspect. Med.* **4**, a013631 (2014).
6. G. Solanas, S. A. Benitah, Regenerating the skin: A task for the heterogeneous stem cell pool and surrounding niche. *Nat. Rev. Mol. Cell Biol.* **14**, 737–748 (2013).
7. M. Ito *et al.*, Stem cells in the hair follicle bulge contribute to wound repair but not to homeostasis of the epidermis. *Nat. Med.* **11**, 1351–1354 (2005).
8. M. E. Page, P. Lombard, F. Ng, B. Göttgens, K. B. Jensen, The epidermis comprises autonomous compartments maintained by distinct stem cell populations. *Cell Stem Cell* **13**, 471–482 (2013).
9. P. Rompolas, K. R. Mesa, V. Greco, Spatial organization within a niche as a determinant of stem-cell fate. *Nature* **502**, 513–518 (2013).
10. F. M. Watt, K. B. Jensen, Epidermal stem cell diversity and quiescence. *EMBO Mol. Med.* **1**, 260–267 (2009).
11. J. G. Rheinwald, H. Green, Formation of a keratinizing epithelium in culture by a cloned cell line derived from a teratoma. *Cell* **6**, 317–330 (1975).
12. C. K. Sen, *et al.* Human skin wounds: A major and snowballing threat to public health and the economy. *Wound Repair Regen.* **17**:763–771 (2009).

13. M. C. Latella *et al.*, Correction of recessive dystrophic epidermolysis bullosa by transposon-mediated integration of COL7A1 in transplantable patient-derived primary keratinocytes. *J. Invest. Dermatol.* **137**, 836–844 (2017).
14. V. Ronfard, J. M. Rives, Y. Neveux, H. Carsin, Y. Barrandon, Long-term regeneration of human epidermis on third degree burns transplanted with autologous cultured epithelium grown on a fibrin matrix. *Transplantation* **70**, 1588–1598 (2000).
15. G. L. Sen, D. E. Webster, D. I. Barragan, H. Y. Chang, P. A. Khavari, Control of differentiation in a self-renewing mammalian tissue by the histone demethylase JMJD3. *Genes Dev.* **22**, 1865–1870 (2008).
16. K. W. Mulder *et al.*, Diverse epigenetic strategies interact to control epidermal differentiation. *Nat. Cell Biol.* **14**, 753–763 (2012).
17. W. Xu *et al.*, Application of a partial-thickness human ex vivo skin culture model in cutaneous wound healing study. *Lab. Invest.* **92**, 584–599 (2012).
18. L. Steinstraesser *et al.*, A human full-skin culture system for interventional studies. *Eplasty* **9**, e5 (2009).
19. S. Ikuta, N. Sekino, T. Hara, Y. Saito, K. Chida, Mouse epidermal keratinocytes in three-dimensional organotypic coculture with dermal fibroblasts form a stratified sheet resembling skin. *Biosci. Biotechnol. Biochem.* **70**, 2669–2675 (2006).
20. S. H. Yuspa, P. Hawley-Nelson, B. Koehler, J. R. Stanley, A survey of transformation markers in differentiating epidermal cell lines in culture. *Cancer Res.* **40**, 4694–4703 (1980).
21. M. R. Romero, J. M. Carroll, F. M. Watt, Analysis of cultured keratinocytes from a transgenic mouse model of psoriasis: Effects of suprabasal integrin expression on keratinocyte adhesion, proliferation and terminal differentiation. *Exp. Dermatol.* **8**, 53–67 (1999).
22. M. Choi, C. Lee, Immortalization of primary keratinocytes and its application to skin research. *Biomol. Ther. (Seoul)* **23**, 391–399 (2015).
23. C. A. Chacón-Martínez, M. Klose, C. Niemann, I. Glauche, S. A. Wickström, Hair follicle stem cell cultures reveal self-organizing plasticity of stem cells and their progeny. *EMBO J.* **36**, 151–164 (2017).
24. M. Lei *et al.*, Self-organization process in newborn skin organoid formation inspires strategy to restore hair regeneration of adult cells. *Proc. Natl. Acad. Sci. U.S.A.* **114**, E7101–E7110 (2017).
25. T. Sato *et al.*, Single Lgr5 stem cells build crypt-villus structures in vitro without a mesenchymal niche. *Nature* **459**, 262–265 (2009).
26. T. Sato *et al.*, Long-term expansion of epithelial organoids from human colon, adenoma, adenocarcinoma, and Barrett's epithelium. *Gastroenterology* **141**, 1762–1772 (2011).
27. K. Kretzschmar, H. Clevers, Organoids: Modeling development and the stem cell niche in a dish. *Dev. Cell* **38**, 590–600 (2016).
28. K. B. Jensen, R. R. Driskell, F. M. Watt, Assaying proliferation and differentiation capacity of stem cells using disaggregated adult mouse epidermis. *Nat. Protoc.* **5**, 898–911 (2010).
29. G. J. Brewer, J. R. Torricelli, E. K. Evege, P. J. Price, Optimized survival of hippocampal neurons in B27-supplemented Neurobasal, a new serum-free medium combination. *J. Neurosci. Res.* **35**, 567–576 (1993).
30. K. Kretzschmar, H. Clevers, Wnt/β-catenin signaling in adult mammalian epithelial stem cells. *Dev. Biol.* **428**, 273–282 (2017).
31. J. G. Rheinwald, H. Green, Epidermal growth factor and the multiplication of cultured human epidermal keratinocytes. *Nature* **265**, 421–424 (1977).
32. V. A. Botchkarev *et al.*, Noggin is required for induction of the hair follicle growth phase in postnatal skin. *FASEB J.* **15**, 2205–2214 (2001).
33. H. Kulessa, G. Turk, B. L. Hogan, Inhibition of Bmp signaling affects growth and differentiation in the anagen hair follicle. *EMBO J.* **19**, 6664–6674 (2000).
34. N. Oshimori, E. Fuchs, Paracrine TGF-β signaling counterbalances BMP-mediated repression in hair follicle stem cell activation. *Cell Stem Cell* **10**, 63–75 (2012).
35. H. Green, Cyclic AMP in relation to proliferation of the epidermal cell: A new view. *Cell* **15**, 801–811 (1978).
36. J. F. Dekkers *et al.*, A functional CFTR assay using primary cystic fibrosis intestinal organoids. *Nat. Med.* **19**, 939–945 (2013).
37. H. Ohuchi *et al.*, FGF10 acts as a major ligand for FGF receptor 2 IIIb in mouse multiorgan development. *Biochem. Biophys. Res. Commun.* **277**, 643–649 (2000).
38. A. Füllgrabe *et al.*, Dynamics of Lgr6$^+$ progenitor cells in the hair follicle, sebaceous gland, and interfollicular epidermis. *Stem Cell Rep.* **5**, 843–855 (2015).
39. K. Kretzschmar, C. Weber, R. R. Driskell, E. Calonje, F. M. Watt, Compartmentalized epidermal activation of β-catenin differentially affects lineage reprogramming and underlies tumor heterogeneity. *Cell Rep.* **14**, 269–281 (2016).
40. V. Jaks *et al.*, Lgr5 marks cycling, yet long-lived, hair follicle stem cells. *Nat. Genet.* **40**, 1291–1299 (2008).
41. H. J. Snippert *et al.*, Lgr6 marks stem cells in the hair follicle that generate all cell lineages of the skin. *Science* **327**, 1385–1389 (2010).
42. N. Barker *et al.*, Identification of stem cells in small intestine and colon by marker gene Lgr5. *Nature* **449**, 1003–1007 (2007).
43. U. B. Jensen *et al.*, A distinct population of clonogenic and multipotent murine follicular keratinocytes residing in the upper isthmus. *J. Cell Sci.* **121**, 609–617 (2008).
44. S. Müller-Röver *et al.*, A comprehensive guide for the accurate classification of murine hair follicles in distinct hair cycle stages. *J. Invest. Dermatol.* **117**, 3–15 (2001).
45. H. D. de Koning *et al.*, Expression profile of cornified envelope structural proteins and keratinocyte differentiation-regulating proteins during skin barrier repair. *Br. J. Dermatol.* **166**, 1245–1254 (2012).
46. P. Rabbani *et al.*, Coordinated activation of Wnt in epithelial and melanocyte stem cells initiates pigmented hair regeneration. *Cell* **145**, 941–955 (2011).
47. C. S. Verissimo *et al.*, Targeting mutant RAS in patient-derived colorectal cancer organoids by combinatorial drug screening. *eLife* **5**, e18489 (2016).
48. J. A. Doudna, E. Charpentier, Genome editing. The new frontier of genome engineering with CRISPR-Cas9. *Science* **346**, 1258096 (2014).
49. N. V. Whittock *et al.*, Compound heterozygosity for non-sense and mis-sense mutations in desmoplakin underlies skin fragility/woolly hair syndrome. *J. Invest. Dermatol.* **118**, 232–238 (2002).
50. V. Vasioukhin, E. Bowers, C. Bauer, L. Degenstein, E. Fuchs, Desmoplakin is essential in epidermal sheet formation. *Nat. Cell Biol.* **3**, 1076–1085 (2001).
51. T. Lechler, E. Fuchs, Desmoplakin: An unexpected regulator of microtubule organization in the epidermis. *J. Cell Biol.* **176**, 147–154 (2007).
52. S. Baum, N. Sakka, O. Artsi, H. Trau, A. Barzilai, Diagnosis and classification of autoimmune blistering diseases. *Autoimmun. Rev.* **13**, 482–489 (2014).
53. J. Chen, Z. Den, P. J. Koch, Loss of desmocollin 3 in mice leads to epidermal blistering. *J. Cell Sci.* **121**, 2844–2849 (2008).
54. S. Joost *et al.*, Single-cell transcriptomics reveals that differentiation and spatial signatures shape epidermal and hair follicle heterogeneity. *Cell Syst.* **3**, 221–237.e9 (2016).
55. O. Basak *et al.*, Induced quiescence of Lgr5$^+$ stem cells in intestinal organoids enables differentiation of hormone-producing enteroendocrine cells. *Cell Stem Cell* **20**, 177–190.e4 (2017).
56. T. Hashimshony *et al.*, CEL-Seq2: Sensitive highly-multiplexed single-cell RNA-seq. *Genome Biol.* **17**, 77 (2016).
57. T. Wang, J. J. Wei, D. M. Sabatini, E. S. Lander, Genetic screens in human cells using the CRISPR-Cas9 system. *Science* **343**, 80–84 (2014).
58. N. E. Sanjana, O. Shalem, F. Zhang, Improved vectors and genome-wide libraries for CRISPR screening. *Nat. Methods* **11**, 783–784 (2014).